Int. J. Heat Mass Transfer. Vol. 36, No. 1, pp. 189–199, 1993
Printed in Great Britain

0017–9310/93 $5.00 + 0.00

Gas absorption and solid dissolution in a thin liquid film on a rotating disk

M. M. RAHMAN† and A. FAGHRI
Department of Mechanical and Materials Engineering, Wright State University, Dayton, OH 45435, U.S.A.

(*Received* 31 *July* 1991 *and in final form* 9 *January* 1992)

Abstract—Analytical and numerical solutions for mass transfer to a thin liquid film adjacent to a horizontal rotating disk are developed for the processes of gas absorption at the free surface and solid dissolution at the disk wall. The analytical approach was derived from a scaling analysis and presented solutions in closed form using confluent hypergeometric functions. The numerical approach solved the full three-dimensional transport equations. In the latter case, the location of the free surface was predicted by an iterative scheme and its irregular shape was preserved by employing a boundary-fitted curvilinear coordinate system for computation. Results are presented in non-dimensional form using Reynolds and Ekman numbers as parameters. It was found that for a given flow system, a significant enhancement of the absorption or dissolution rate can be achieved by increasing the angular velocity of the disk.

INTRODUCTION

THE PRESENT study was primarily motivated by the idea of a compact, lightweight absorber unit for heat pumps to be used in space vehicles. The crucial feature of this design is to attain a large rate of absorption of the refrigerant vapor to the absorbent in a small amount of space where the gravitational body force is practically zero. The idea proposed is to discharge the absorbent as a thin film onto a rotating disk where it will be carried by inertial and centrifugal forces. A large transport rate will be obtained as is typical in gravity-driven thin film columns used commonly in process industries. The added advantage of a rotating unit is that at a relatively large rate of rotation, its performance is identical on earth and in space. Therefore, the unit can be tested on earth before its installation in a space-bound vehicle. The present study approaches this gas absorption process in a fundamental way and, in addition, presents the phenomenon of solid dissolution which has important applications in chemical process industries.

Mass transfer in a thin liquid film has been quite extensively studied for a film falling along a vertical or inclined surface under the action of gravity. Olbrich and Wild [1] developed an analytical solution for the diffusion of a gas from the free surface to the liquid film using a Laplace transform. The laminar flows over a sphere, cone or cycloid of revolution were considered. Boyadjiev [2] presented an analytical solution to the non-linear mass transfer problem when gas absorption takes place on the free surface of a laminar liquid film undergoing a first-order chemical reaction. The method of separation of variables was used by Riazi and Faghri [3] to investigate the problem of gas absorption to a falling film with a zero-order homogeneous reaction. Solutions were obtained in terms of confluent hypergeometric functions. The effect of interfacial drag on the rate of gas absorption in the presence of a chemical reaction was investigated by Riazi and Faghri [4]. The process of solid dissolution to a thin solvent film was considered by Riazi and Faghri [5]. Assuming laminar flow with constant fluid properties, the effects of chemical reaction on the rate of dissolution were investigated analytically. Coupled heat and mass transfer to a turbulent falling film was studied by Grossman and Heath [6] and Faghri and Seban [7, 8]. Analytical and numerical values of the Sherwood number were obtained for different values of Reynolds and Schmidt numbers.

Mass transfer to a thin film adjacent to a rotating surface was studied primarily in relation to rotating disk contactors and polymer processing equipment. Suga and Boongorsrang [9] developed a model for mass transfer to a thin liquid film on a vertically spinning disk in a rotating disk contactor unit. The disk was half immersed in the liquid medium and oxygen was transferred from the ambient air to the liquid via the thin film. Vaidya and Pangarkar [10] developed an analytical model to predict the mass transfer rate in rotating biological contactors when the liquid medium is, in general, non-Newtonian in nature. Bornside *et al.* [11] developed a one-dimensional model for the spin coating process including the variations of concentration, viscosity and diffusivity across the thickness of the spin coated film. The equations for flow and mass diffusion were solved numerically.

The phenomenon of gas absorption or solid dissolution in a thin liquid film discharged from a pres-

† Present address: Mainstream Engineering Corporation, 200 Yellow Place, Rockledge, FL 32955, U.S.A.

NOMENCLATURE

C	mass concentration [kg of component/kg of mixture]
D	mass diffusivity [$m^2 s^{-1}$]
E	Ekman number, $\nu/\omega r^2$
$\mathbf{g}$	gravitational acceleration, $9.81\mathbf{j}$ [$m s^{-2}$]
G	mass transfer coefficient: $m_0/(C_0-C_m)$, for gas absorption; $m_w/(C_w-C_m)$, for solid dissolution [$kg m^{-2} s^{-1}$]
$\mathbf{i}$	unit vector in the angular direction
$\mathbf{j}$	unit vector in the direction normal to the plate
$\mathbf{k}$	unit vector in the z-direction
m	mass flux [$kg m^{-2} s^{-1}$]
n	coordinate normal to the free surface [m]
$\mathbf{n}$	unit vector normal to the free surface
p	static pressure [Pa]
Q	volumetric flow rate [$m^3 s^{-1}$]
r	radial coordinate [m]
Re	Reynolds number, $W\delta/\nu$
Sc	Schmidt number, ν/D
Sh	Sherwood number, $[G(\nu^2/g)^{1/3}]/\rho D$
Sh^*	Sherwood number in terms of film height, $G\delta/\rho D$
t	time [s]
$\mathbf{t}$	unit vector tangential to the free surface
u	velocity in the angular direction [$m s^{-1}$]
v	velocity in the direction normal to the plate [$m s^{-1}$]
$\mathbf{V}$	velocity vector [$m s^{-1}$]
w	velocity in the z-direction [$m s^{-1}$]
W	average velocity along the radius [$m s^{-1}$]
y	coordinate normal to the plate [m]
Y	dimensionless coordinate normal to the plate, y/δ
z	coordinate in the radial flow direction [m]
Z	dimensionless radial coordinate defined by equation (15d).

Greek symbols

δ	film thickness [m]
δ^+	dimensionless film thickness, δ/r_{in}
θ	angular coordinate [rad]
λ	eigenvalue
ν	kinematic viscosity [$m^2 s^{-1}$]
ξ	dimensionless radial coordinate, r/r_{in}
ρ	density [$kg m^{-3}$]
τ	stress tensor [$N m^{-2}$]
ψ	dimensionless concentration defined by equation (15a)
ω	angular velocity [$rad s^{-1}$].

Subscripts

b	mixed-mean (bulk) condition
in	condition at entrance
0	condition on free surface
out	condition at exit
w	condition on solid wall.

surized source at the center of a horizontal rotating disk has not been studied in any previous work. This kind of system is significantly different from a vertical disk contactor or spin coating machine in that the fluid is carried by the combined effects of the inertial and centrifugal forces. The fluid flow and heat transfer in this kind of system were investigated recently by Thomas *et al.* [12, 13] and Rahman and Faghri [14].

Thomas *et al.* [12] developed a one-dimensional numerical model for the prediction of film height by integrating the equations for the conservation of mass and momentum across the thickness of the film. Results were presented for different values of Reynolds and Rossby numbers. Thomas *et al.* [13] presented experimental data for the film height distribution and a photographic study of surface waves at different flow rates and rotational speeds. No measurement of heat or mass transfer coefficients was attempted in that study. A complete three-dimensional solution algorithm for fluid flow adjacent to a rotating disk was developed by Rahman and Faghri [14]. Computations were performed for different flow rates and rotational speeds using a curvilinear boundary fitted coordinate system. The free surface of the film conformed to one of the boundaries of the computation domain. An iterative solution procedure was developed to determine the free surface height distribution that was dependent on flow rate, angular velocity and other parameters. The computed results agreed very well with the experimental measurements of Thomas *et al.* [13]. The main objective of that study was to numerically determine the flow field and associated film height distribution. Some heat transfer results were also presented.

The present study has the following objectives:

(1) To extend the free surface computational procedure developed by Rahman and Faghri [14] to study the processes of gas absorption and solid dissolution in a liquid film formed by a controlled liquid jet on a rotating disk.

(2) To develop analytical solutions for the above processes.

(3) To predict the performance of a typical rotating disk unit such as that used by Thomas *et al.* [13] under different flow rates and rates of rotation.

EQUATIONS OF TRANSPORT

The equations governing the conservation of mass, momentum, and species concentration for the steady,

incompressible, laminar flow of a thin film of a Newtonian, constant-property liquid can be written as

$$\nabla \cdot \mathbf{V} = 0 \tag{1}$$

$$\frac{D\mathbf{V}}{Dt} = -\frac{1}{\rho}\nabla p + \nu \nabla^2 \mathbf{V} + \mathbf{g} \tag{2}$$

$$\frac{DC}{Dt} = D\nabla^2 C. \tag{3}$$

The present flow system is shown schematically in Fig. 1. Fluid is discharged axisymmetrically at a radial location $r = r_{in}$ on a disk rotating with a constant angular velocity ω about its axis. A moving coordinate system attached to the free surface is used for analysis and computation. The boundary conditions are given by

at the free surface ($y = 0$):

$$\tau \cdot \mathbf{n} = 0, \quad \tau \cdot \mathbf{t} = 0, \quad \frac{d\delta}{dr} = -\frac{v}{w},$$

$$\begin{cases} C = C_0 & \text{for gas absorption} \\ \dfrac{\partial C}{\partial n} = 0 & \text{for solid dissolution} \end{cases} \tag{4}$$

at the disk surface ($y = \delta$):

$$\mathbf{V} = \omega r \mathbf{i}, \quad \begin{cases} \dfrac{\partial C}{\partial y} = 0 & \text{for gas absorption} \\ C = C_w & \text{for solid dissolution} \end{cases} \tag{5}$$

at the entrance ($r = r_{in}$):

$$\mathbf{V} = 1.5 W_{in}\left[1 - \left(\frac{y}{\delta}\right)^2\right]\mathbf{k}, \quad C = C_{in} \tag{6}$$

at the exit ($r = r_{out}$):

$$\frac{\partial \mathbf{V}}{\partial z} = 0, \quad \frac{\partial p}{\partial y} = \rho g, \quad \frac{\partial C}{\partial z} = 0. \tag{7}$$

Due to the axisymmetric nature of the flow, there is no variation of velocity or concentration in the angular direction. At the free surface the streamline condition needs to be satisfied, which is appropriate when the rate of gas absorption at the free surface is small. The surface tension on the free surface is small (Weber number is large). The effects of interfacial waves at the free surface of the liquid are also assumed to be negligible. Under this condition, the vanishing normal stress conditions can be imposed in a simplified form as a balance between the free surface and ambient pressures. At the entrance plane, the flow is assumed to have a parabolic profile as is typical for a free surface flow. At the exit plane the flow is assumed to be fully-developed with a hydrostatic pressure profile. The concentration profile is also assumed to approach a fully-developed condition at that location. In the case of gas absorption at the free surface, the concentration gradient vanishes at the solid wall due to the impermeable nature of the wall. For the solid dissolution process, the rate of mass transfer at the wall is assumed to be small enough to avoid any change in flow rate, as well as in the size or shape of the disk. There is no diffusion at the free surface during this process.

In addition to the geometric parameters pertaining to the physical system, the dimensionless groups that are significant for thin film flows over a rotating disk are the Reynolds, Ekman, Schmidt and Sherwood numbers. The Reynolds and Ekman numbers quantify the driving mechanisms for the flow, namely, inertial and centrifugal forces. The most significant length scale that controls the transport processes is the film thickness δ. The Sherwood number defined using the film thickness as the length scale is denoted as Sh^*. Since δ varies along the radius of the disk, an alternative definition of the Sherwood number using $(\nu^2/g)^{1/3}$ as the length scale is also used to present the variation of the mass transfer coefficient. This latter length scale is commonly used in the thin falling film literature.

ANALYTICAL APPROACH

The cylindrical coordinate system (r–θ–y) shown in Fig. 1 was used for the development of an analytical

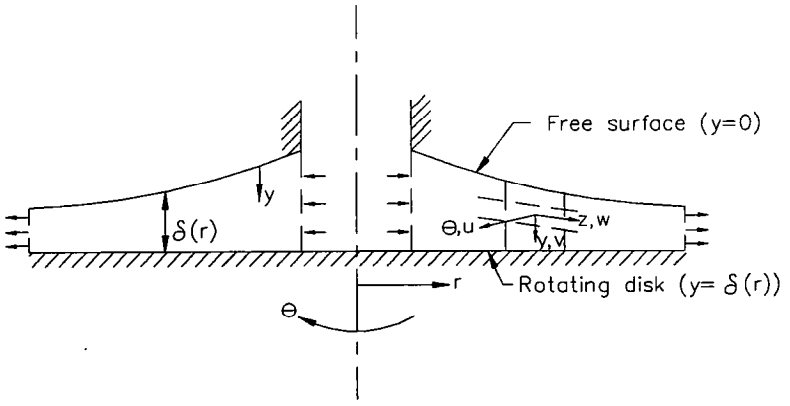

FIG. 1. Schematic of the flow and coordinate systems.

solution. The r-axis is directed along the radius of the disk and the θ-axis is in the azimuthal direction. The y-axis is perpendicular to the disk with its origin on the free surface. The following assumptions are made to simplify the problem for the analytical solution.

(1) $v \ll u$ or w and $\partial/\partial y \gg \partial/\partial r$. These assumptions are valid since the thickness of the film is much smaller than the radius of the disk.

(2) $p \approx$ constant. In the absence of any significant hydrostatic pressure variation, the pressure everywhere in the film is equal to the ambient pressure.

(3) $g/\omega^2 r \ll 1$. The gravitational body force is an order of magnitude smaller than the centrifugal force even for a moderate rate of rotation. This assumption was verified by the numerical solution. Computations with $g = 0.0$ and 9.81 m s^{-2} yielded results to within 0.01%.

(4) $w \ll u$ and $u = \omega r$. These assumptions are true only at a large rate of rotation, and become more appropriate at larger radii.

The momentum and concentration equations then reduce to the following form:

$$\frac{d^2w}{dy^2} = -\frac{\omega^2 r}{v} \tag{8}$$

$$w\frac{\partial C}{\partial r} = D\frac{\partial^2 C}{\partial y^2}. \tag{9}$$

Integrating equation (8) and using the appropriate boundary conditions (at $y = 0$, $dw/dy = 0$; and at $y = \delta$, $w = 0$), the following expression for the local velocity distribution is obtained:

$$w = \frac{\omega^2 r\delta^2}{2v}\left[1 - \left(\frac{y}{\delta}\right)^2\right]. \tag{10}$$

The average velocity at any radial location can be determined by integrating the local velocity across the thickness of the film:

$$W = \frac{\omega^2 r\delta^2}{3v}. \tag{11}$$

The conservation of mass at any radial location can be written as

$$Q = 2\pi r W\delta. \tag{12}$$

The solution of equations (11) and (12) gives the film height distribution as

$$\delta = \left(\frac{3vQ}{2\pi\omega^2 r^2}\right)^{1/3}. \tag{13}$$

Substituting the fluid flow results from equations (10) to (13) into equation (9) and non-dimensionalizing, the transport equation becomes

$$(1 - Y^2)\frac{\partial\psi}{\partial Z} = \frac{\partial^2\psi}{\partial Y^2} \tag{14}$$

where

$$\psi = \begin{cases} \dfrac{C_0 - C}{C_0 - C_{in}} & \text{for gas absorption} \\ \dfrac{C_w - C}{C_w - C_{in}} & \text{for solid dissolution} \end{cases} \tag{15a}$$

$$Y = \frac{y}{\delta} \tag{15b}$$

$$\xi = \frac{r}{r_{in}} \tag{15c}$$

and

$$Z = 0.1733 Re_{in}^{-4/3} E_{in}^{-2/3} Sc^{-1}[\xi^{8/3} - 1]. \tag{15d}$$

The boundary conditions (4)–(6) can be expressed as

$$\text{at} \quad Y = 0: \quad \begin{cases} \psi = 0 & \text{for gas absorption} \quad (16a) \\ \dfrac{\partial\psi}{\partial Y} = 0 & \text{for solid dissolution} \quad (16b) \end{cases}$$

$$\text{at} \quad Y = 1: \quad \begin{cases} \dfrac{\partial\psi}{\partial Y} = 0 & \text{for gas absorption} \quad (17a) \\ \psi = 0 & \text{for solid dissolution} \quad (17b) \end{cases}$$

$$\text{at} \quad Z = 0: \quad \psi = 1. \tag{18}$$

The method of separation of variables was used to solve equation (14) along with the boundary conditions (16)–(18) for the two transport processes considered here.

Gas absorption

Substituting $\psi(Z, Y) = \hat{M}(Z)\hat{N}(Y)$ into equation (14), the solutions for the resulting ordinary differential equations were obtained as

$$\hat{M} = C_1 \exp(-\lambda^2 Z) \tag{19a}$$

$$\hat{N} = C_2 \exp(-\lambda Y^2/2) M\left(\frac{1-\lambda}{4}, \frac{1}{2}, \lambda Y^2\right) + C_3 \exp(-\lambda Y^2/2)\lambda^{1/2} Y M\left(\frac{3-\lambda}{4}, \frac{3}{2}, \lambda Y^2\right) \tag{19b}$$

where $M(a, b, c)$ is the confluent hypergeometric function with arguments a, b and c [15]. In this process, the equation with $\hat{N}$ as the dependent variable was reduced to Kummer's equation by the substitution of $p = \lambda Y^2$ and $Q = \hat{N}\exp(p/2)$. The solution could then be readily expressed in terms of confluent hypergeometric functions.

Substitution of the boundary conditions (at $Y = 0$: $\hat{N} = 0$; and at $Y = 1$: $d\hat{N}/dY = 0$) into equation (19b) gives the characteristic equation in the form:

$$(1-\lambda_n) M\left(\frac{3-\lambda_n}{4}, \frac{3}{2}, \lambda_n\right) + \frac{\lambda_n(3-\lambda_n)}{3} M\left(\frac{7-\lambda_n}{4}, \frac{5}{2}, \lambda_n\right) = 0. \tag{20}$$

The roots of this equation give the eigenvalues. The

solution for concentration distribution can be written as

$$\psi(Z, Y) = \sum_{n=1}^{\infty} C_n \exp(-\lambda_n^2 Z) \times \exp(-\lambda_n Y^2/2)\lambda_n^{1/2} YM\left(\frac{3-\lambda_n}{4}, \frac{3}{2}, \lambda_n Y^2\right). \quad (21)$$

The use of boundary condition (18) in equation (21) gives the eigenfunctions as

$$Y_n(Y) = \exp(-\lambda_n Y^2/2)\lambda_n^{1/2} YM\left(\frac{3-\lambda_n}{4}, \frac{3}{2}, \lambda_n Y^2\right). \quad (22)$$

The values of C_n were determined by using the orthogonal property of eigenfunctions:

$$C_n = \frac{\int_0^1 (1-Y^2) Y_n \, dY}{\int_0^1 (1-Y^2) Y_n^2 \, dY}. \quad (23)$$

The first 15 values of λ_n and C_n are listed in Table 1. λ_n was determined by solving equation (20) using the bisection method [16]. C_n was obtained from equations (22) and (23) for the corresponding value of λ_n. The integration was performed numerically using Simpson's rule [16]. Due to the periodic nature of confluent hypergeometric functions, the solution was found to be sensitive to truncation errors. Therefore, 32 significant digits were retained for all mathematical operations and 1000 intervals were used for the integration. Both λ_n and C_n were in agreement with the previous solution of Olbrich and Wild [1], who investigated gas diffusion in a falling liquid film.

The Sherwood number for gas absorption can be obtained by evaluating the concentration gradient at the free surface and the average concentration across the film thickness using equation (21). This results in

$$Sh^* = \frac{\sum_{n=1}^{\infty} C_n \exp(-\lambda_n^2 Z)\lambda_n^{1/2} M\left(\frac{3-\lambda_n}{4}, \frac{3}{2}, \lambda_n Y^2\right)}{\sum_{n=1}^{\infty} C_n \exp(-\lambda_n^2 Z)\lambda_n^{1/2} \times \int_0^1 \exp(-\lambda_n Y^2/2) YM\left(\frac{3-\lambda_n}{4}, \frac{3}{2}, \lambda_n Y^2\right) dY}. \quad (24)$$

Solid dissolution

The resulting ordinary differential equations for solid dissolution were solved in a way analogous to that for gas absorption. The characteristic equation for solid dissolution was found to be

$$M\left(\frac{1-\lambda_n}{4}, \frac{1}{2}, \lambda_n\right) = 0. \quad (25)$$

The roots of this equation give the eigenvalues λ_n. The first 15 eigenvalues are listed in Table 2.

The concentration distribution was represented by the equation

$$\psi(Z, Y) = \sum_{n=1}^{\infty} C_n \exp(-\lambda_n^2 Z) \times \exp(-\lambda_n Y^2/2) M\left(\frac{1-\lambda_n}{4}, \frac{1}{2}, \lambda_n Y^2\right). \quad (26)$$

The eigenfunctions were found to be

$$Y_n(Y) = \exp(-\lambda_n Y^2/2) M\left(\frac{1-\lambda_n}{4}, \frac{1}{2}, \lambda_n Y^2\right). \quad (27)$$

The values of C_n were determined using these eigenfunctions in equation (23) and carrying out the integration using Simpson's rule. The results are listed in Table 2.

The Sherwood number for solid dissolution can be expressed as

Table 1. Eigenvalues and eigenfunctions for gas absorption to a thin liquid film on a rotating disk

n	λ_n	C_n
1	2.26311054	1.79238363
2	6.29768520	1.02469024
3	10.30772682	0.7963124
4	14.31279359	0.67455968
5	18.31592741	0.59583223
6	22.31808871	0.53954481
7	26.31968464	0.49671463
8	30.32091973	0.46270679
9	34.32190893	0.43485375
10	38.32272220	0.41149662
11	42.32340476	0.39154218
12	46.32398727	0.37423667
13	50.32449130	0.35904122
14	54.32493249	0.34555900
15	58.32532250	0.33349040

Table 2. Eigenvalues and eigenfunctions for solid dissolution to a thin liquid film on a rotating disk

n	λ_n	C_n
1	1.68159532	−1.20083833
2	5.66985735	0.29921538
3	9.66824246	−0.16079095
4	13.66766144	0.10748358
5	17.66737357	−0.07960705
6	21.66720532	0.06280738
7	25.66709649	−0.05147898
8	29.66702104	0.04355501
9	33.66696607	−0.03750097
10	37.66692446	0.03297711
11	41.66689201	−0.02923400
12	45.66686609	0.02634957
13	49.66684497	−0.02380988
14	53.66682747	0.02183381
15	55.66681278	−0.01999587

$$Sh^* = \frac{\sum_{n=1}^{\infty} C_n \exp(-\lambda_n^2 Z)\exp(-\lambda_n/2)\lambda_n \times \left[(1-\lambda_n)M\left(\frac{5-\lambda_n}{4}, \frac{3}{2}, \lambda_n\right) - M\left(\frac{1-\lambda_n}{4}, \frac{1}{2}, \lambda_n\right)\right]}{\sum_{n=1}^{\infty} C_n \exp(-\lambda_n^2 Z)\int_0^1 \exp(-\lambda_n Y^2/2) \times M\left(\frac{1-\lambda_n}{4}, \frac{1}{2}, \lambda_n Y^2\right) dY} \quad (28)$$

The variation of the mass transfer coefficient, which was represented by Sh, can be related to Sh^* by the expression

$$Sh = Sh^* \, A \, Re_{in}^{-1/3} \, E_{in}^{-2/3} \, \xi^{2/3} \quad (29)$$

where

$$A = \left(\frac{\nu^2}{3gr_{in}^3}\right)^{1/3}.$$

Since the film thickness changes along the radius of the disk, this latter quantity was calculated to get a better understanding of how the absorption or dissolution rate changes with flow rate and rate of rotation.

FULL NUMERICAL SIMULATION

The numerical simulation of the transport processes was carried out by solving the equations of motion and transport (1)–(3) along with boundary conditions (4)–(7) using the boundary-fitted curvilinear coordinate system illustrated in Fig. 1. The irregular free surface was taken as one of the boundaries of the computation domain. Computation was done for a pie-shaped flow domain extending from r_{in} to r_{out} in the radial direction and over a small angle in the angular direction in order to prevent both distortion of body-fitted coordinates at larger radii and clustering of grids at smaller radii. The grid cells were generated by an algebraic interpolation between the boundaries of the domain. In general, the cell faces were non-orthogonal to each other. The local coordinates were defined along lines connecting the centers of the adjacent grid cells. The θ-axis was directed in the azimuthal direction, the y-axis was perpendicular to the plate, and the z-axis was in the radial flow direction. The velocity resolutes in these three directions are u, v and w, respectively. The discretization was done using the finite-volume formulation [17], where the conservation equations were integrated for each cell. The relative importance of convection and diffusion was determined from the magnitude of the local Peclet number, and the diffusion contribution was retained according to the hybrid difference scheme. The flow field was solved by using the SIMPLEST algorithm [18]. The convergence was monitored by checking field values at specific locations where large changes were expected, as well as by checking the sum of the residuals of the governing equations for the entire flow field. Acceptable solutions corresponded to invariant spot values to the fourth decimal place as well as residuals of less than 10^{-6} for each equation.

The number of grid cells required for the computation was determined from a series of tests by gradually increasing the number of cells in each coordinate direction. It was found that the computed distributions of film height and mass transfer coefficient converge to a single solution when the number of cells is sufficient. In the radial direction, 45 and 50 cells yielded identical results. In the direction normal to the plate, 30 cells were found to be adequate. Due to the axisymmetric nature of the flow, only five cells with an angular extent of 2.3°/cell were found to be adequate in the θ-direction. This provided a total angle of 11.5° for the entire pie-shaped computational domain. Test runs with 3.45°/cell and 2.3°/cell yielded Sherwood numbers to within 0.001%. Similarly, runs with two cells and five cells in the angular direction resulted in Sherwood numbers to within 0.0005%. Therefore, the computational domain was divided into $50 \times 30 \times 5$ cells in the radial, normal and azimuthal directions respectively by a simple algebraic interpolation to generate the grid structure.

The location of the free surface was found by an iterative procedure where only the mass and momentum conservation equations were solved. The details of this method are given in Rahman and Faghri [14]. During the iteration process, the free surface was assumed to be a porous wall through which fluid particles cross depending on the difference between local and ambient pressures. An outflow took place when the fluid pressure was higher than the ambient and vice versa. Successive improvements of the film height distribution were obtained from the local rate of penetration, and iterations were continued until the rate of penetration became negligible. At this condition, the free surface also formed a streamline. Once the location of the free surface was determined, the concentration equation was solved with the appropriate boundary conditions for the different transport problems considered here.

RESULTS AND DISCUSSION

The analytical and full numerical solution methods described in the previous sections were used to calculate the film height and transport coefficients for some specific combination of flow rates and rates of rotation. Water at 20°C was used to determine the fluid properties. The absorption of carbon dioxide to a water film was considered for the gas absorption problem, where the Schmidt number was $Sc = 559$ [19]. For the dissolution problem, the solid wall was assumed to be made of sucrose, giving a Schmidt number of $Sc = 2230$ [19]. The results corresponding

to the analytical and numerical solutions are compared in Figs. 2–4. The dimensionless parameters used for the presentation of results are the radial location ξ, the film thickness δ^+, the concentration ψ, the Reynolds number Re, and the Ekman number E.

The variations of film thickness along the radius of the disk for two different Ekman numbers for $Re_{in} = 520$ are shown in Fig. 2. The numerical solution, which simulates the flow in an exact fashion, shows that the film height increases from the entrance location, attains a peak and then monotonically decreases downstream. The increase in film height near the entrance is due to frictional resistance from the wall, which overcomes the inertial and centrifugal forces in that region, and decreases the flow velocity. The centrifugal force, however, increases with radius and overcomes the frictional resistance at larger radii, which results in a net acceleration of the film. The film thickness consequently decreases in that region. The analytical solution, which ignores the effects of inertia and assumes solid-body rotation, predicts a monotonic decrease in film height. Also, at larger radii the numerical solution approaches the analytical solution since the effects of inertia decrease and the flow becomes primarily driven by the centrifugal force. As expected, the flow becomes centrifugally driven at small radii when the rotational speed is larger, i.e. smaller Ekman number.

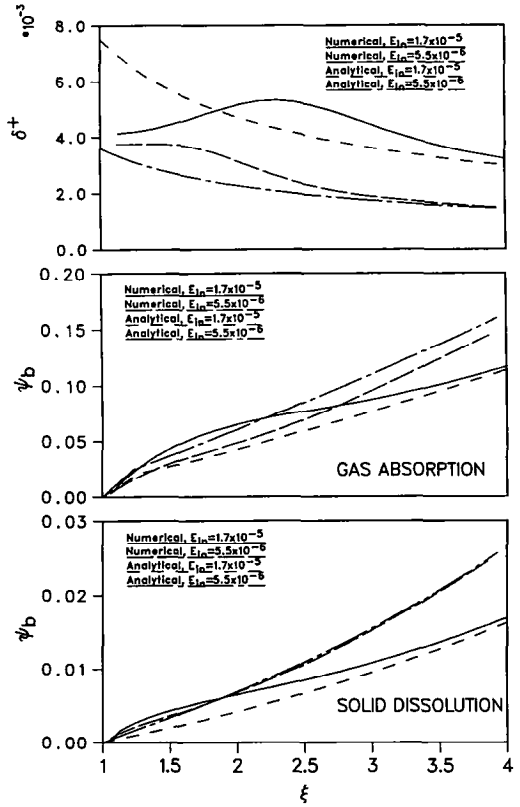

FIG. 2. Comparison of film height variation and mixed-mean concentration for flow over a rotating disk at $Re_{in} = 520$.

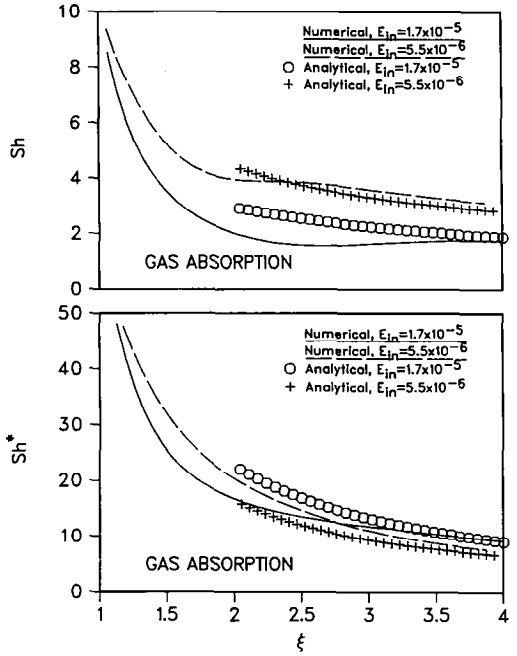

FIG. 3. Comparison of Sherwood number variation for flow over a rotating disk at $Re_{in} = 520$.

Figure 2 also shows the variation of mixed-mean or bulk concentration as a function of radius for both the processes of gas absorption and solid dissolution. As expected, the concentration increases downstream as mass is diffused into the fluid. Here, we also get a better agreement at larger radial locations. The figure

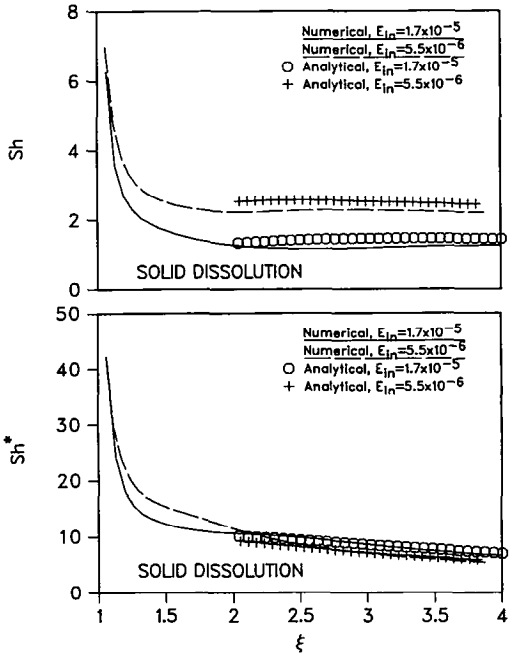

FIG. 4. Comparison of Sherwood number variation for flow over a rotating disk at $Re_{in} = 520$.

also shows an increase of the rate of diffusion with rate of rotation, particularly at larger radial locations.

Figure 3 shows the variation of Sherwood number (Sh and Sh^*) for the process of gas absorption for a given Reynolds number and two different Ekman numbers. The rapid decrease of Sherwood number near the entrance is due to the development of the concentration boundary layer. Both analytical and numerical solutions show that Sh^* decreases monotonically downstream. The smaller value of Sh^* for a smaller Ekman number at large radii is due to the smaller film thickness. As expected, the actual mass transfer coefficient becomes larger at smaller Ekman numbers, which can be seen in the distribution of Sh. The analytical solution shows a monotonic decrease in the gas absorption coefficient, whereas the numerical solution shows a minimum at an intermediate location of the flow. The minimum transport coefficient corresponds to the maximum in the film thickness. It can also be noticed that the numerical and analytical solutions compare well at larger radial locations. This is due to the fact that the analytical solution uses the fully-developed film height distribution, which can be approached only at larger radii. At smaller radii, the flow has a significant amount of inertia which affects the associated transport phenomena.

The distributions of Sh and Sh^* for the process of solid dissolution are shown in Fig. 4. The rapid decrease of Sherwood number near the entrance is again due to the development of the concentration boundary layer for the component dissolving from the wall. The analytical and numerical solutions both show Sh^* monotonically decreasing downstream and Sh becoming approximately constant after some radial distance. The increase of mass transfer with rate of rotation is also evident in the distribution of Sh when the results for two different Ekman numbers are compared. Since the process of solid dissolution involves a large Schmidt number, the thickness of the concentration boundary layer is much smaller compared to the momentum boundary layer, and a very large distance is required to approach a fully-developed mass diffusion condition. In a fully-developed region Sh^* may approach a constant value and Sh may increase downstream, which is expected since centrifugal force increases with radius.

Having established the validity of the numerical and analytical approaches from a relative comparison, a parametric study of gas absorption and solid dissolution processes was performed using the Reynolds and Ekman numbers as parameters. The simulated system corresponded to the disk unit used by Thomas *et al.* [13] for experimental measurements of film height and flow visualization. A horizontal disk 406.4 mm in diameter was used for the experiment where water at 20°C was introduced radially through a slot 0.267 mm in height at a radial location of 50.8 mm. The film height distribution along the radius was measured by using a non-obtrusive capacitance probe from 76.2 mm to 195.6 mm. Twenty sets of experimental data were taken covering flow rates of 7–15 l.p.m. and rotational speeds of 55–300 r.p.m. The flow was isothermal and no measurement of heat or mass transfer was done in that experiment. The specific experimental runs chosen for numerical simulation (cases 1–6) are listed in Table 3. Prediction of heat and mass transfer could be done for all the experimental conditions. However, some specific cases covering the range of experiments in terms of flow rate and rate of rotation were selected to understand the transport phenomena efficiently with a limited amount of computational effort. Table 3 also lists some runs (cases 7–9) for which experiments were not performed. The numerical computations of these cases were done to understand the behavior of the flow and transport under an extended range of operating conditions. The flow entered the computation domain at a radial location of $r_{in} = 76.2$ mm. This corresponded to the location where experimental measurements were started. The measured film height at that location corresponded to the inlet film height (δ_{in}) for numerical simulation. For cases 7–9, δ_{in} was assumed to be 0.3 mm, which was approximately an average of the measured height at that location for different flow rates and rates of rotation. The radial velocity profile at that location was assumed to be parabolic in nature with zero at the wall and maximum at the free surface. The fluid was at a uniform temperature of 20°C. The rate of mass transfer during absorption and dissolution was very small compared to the fluid flow rate. Also, the heats of absorption and dissolution were negligible. Therefore, fluid properties remained practically constant during the transport processes.

The variation of film height and dimensionless mixed mean concentration for the processes of gas absorption and solid dissolution are shown in Fig. 5 for the cases considered in Table 3. At large Ekman numbers (i.e. small rates of rotation), the film height monotonically increases downstream. On the other hand, at small Ekman numbers, the film height monotonically decreases downstream. This can be explained from the relative magnitudes of viscous resistance and centrifugal force in the definition of the Ekman number. At intermediate Ekman numbers, the film height increases, attains a peak and then decreases

Table 3. Flow parameter specifications for the study of gas absorption and solid dissolution to a thin liquid film

Case	Flow rate (l.p.m.)	Rotational speed (r.p.m.)	Reynolds number (Re_{in})	Ekman number (E_{in})
1	15	55	520	3.0×10^{-5}
2	15	100	520	1.7×10^{-5}
3	15	200	520	8.3×10^{-6}
4	15	300	520	5.5×10^{-6}
5	11	100	380	1.7×10^{-5}
6	7	100	240	1.7×10^{-5}
7	3	100	100	1.7×10^{-5}
8	30	100	1040	1.7×10^{-5}
9	15	600	520	2.8×10^{-6}

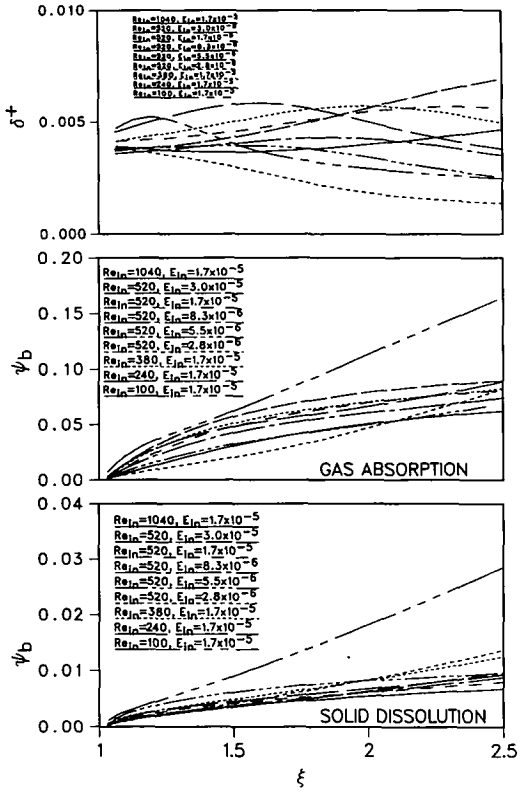

FIG. 5. Numerically predicted film height variation and mixed-mean concentration for flow over a rotating disk.

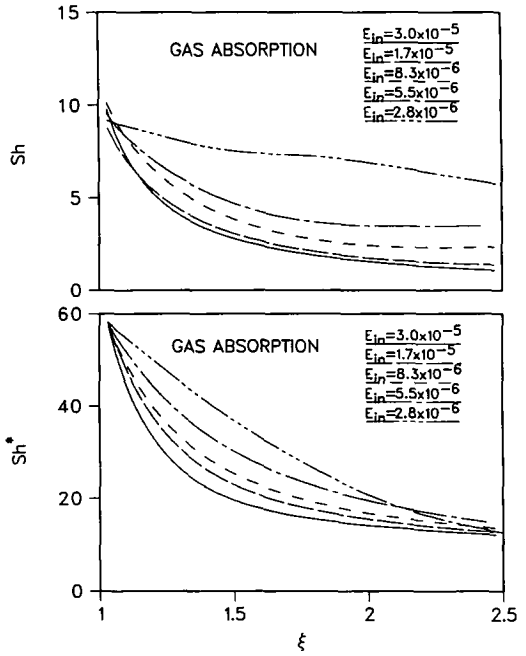

FIG. 6. Numerically predicted Sherwood number variation for flow over a rotating disk at $Re_{in} = 520$.

downstream. As expected, the mixed mean concentration increases with ξ at all values of Reynolds and Ekman numbers.

The variation of Sherwood number for the case of gas absorption at the free surface is demonstrated in Figs. 6 and 7. With a decrease of Ekman number, both *Sh* and *Sh** increase at most locations of the disk. By increasing the rotational speed by a factor of three, the rate of gas absorption can be approximately doubled. From Fig. 7 it can be noticed that a larger mass transfer coefficient can be attained by increasing the Reynolds number only at smaller radii, but an opposite trend is seen at larger radii. As demonstrated by Rahman and Faghri [14], the flow over a rotating disk is dominated by the inertial force at smaller radii and by centrifugal force at larger radii. The mass transfer coefficient increases with Reynolds number only in the inertia-dominated region. At larger radii, a larger mass diffusion rate may be attained for a smaller flow rate since the film becomes thinner, and the local velocity of the film becomes larger for a given rate of rotation. The extent of the inertia-dominated flow increases with Reynolds number, and spans all across the present disk unit only at $Re_{in} = 1040$.

The distribution of Sherwood number for the case of solid dissolution at the wall is plotted in Figs. 8 and 9 for different flow rates and rates of rotation. As expected, the mass transfer coefficient is large near the entrance and decreases slowly downstream. The rate of mass transfer can be significantly increased by increasing the rotational speed (i.e. decreasing the Ekman number). Also, the distribution of Sherwood number is more strongly affected by Ekman number than Reynolds number. Figures 6–9 demonstrate the variation of local mass transfer coefficients. Considering the average mass transfer coefficient for the entire disk, it was found that for the range of con-

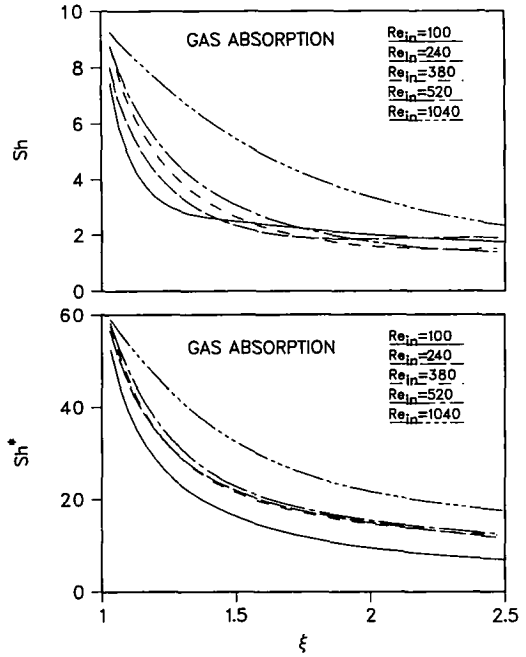

FIG. 7. Numerically predicted Sherwood number variation for flow over a rotating disk at $E_{in} = 1.7 \times 10^{-5}$.

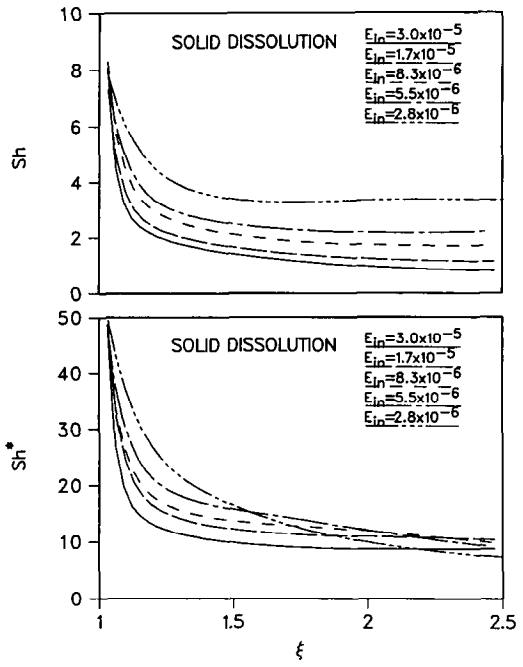

FIG. 8. Numerically predicted Sherwood number variation for flow over a rotating disk at $Re_{in} = 520$.

ditions considered here an overall enhancement of gas absorption as well as solid dissolution are attained both with flow rate and rate of rotation.

CONCLUSIONS

Analytically and numerically calculated mass transfer coefficients during the processes of gas absorption and solid dissolution are presented for the free surface flow of a thin liquid film adjacent to a horizontal rotating disk. The numerical solution simulated the flow and transport using the complete governing equations, whereas the analytical approach solved reduced equations keeping only the most important terms and yielded closed-form solutions in terms of confluent hypergeometric functions. The mass transfer coefficient decreased gradually from a large value near the entrance due to the development of a concentration boundary layer starting at the entrance section. All transport phenomena were dominated by inertia and viscous resistance at smaller radii and by rotation at larger radii. An enhancement of the mass transfer coefficient with flow rate was limited to only the inertia-dominated region. However, a large enhancement spanning over the entire radius was obtained by increasing the rotational speed. This suggests that rotation can be an effective means for the augmentation of the absorption rate of gas to a thin film or the dissolution rate of a solid to a liquid film in chemical process equipment.

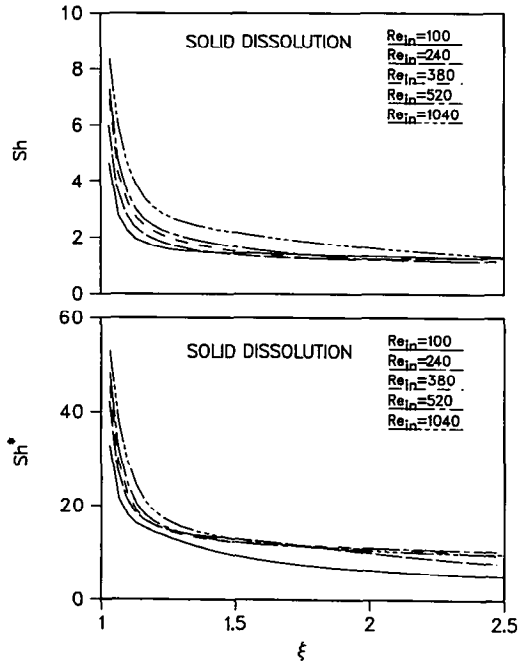

FIG. 9. Numerically predicted Sherwood number variation for flow over a rotating disk at $E_{in} = 1.7 \times 10^{-5}$.

REFERENCES

1. W. E. Olbrich and J. D. Wild, Diffusion from the free surface into a liquid film in laminar flow over defined shapes, *Chem. Engng Sci.* **24,** 25–32 (1969).
2. C. Boyadjiev, Non-linear mass transfer in falling films, *Int. J. Heat Mass Transfer* **25,** 535–540 (1982).
3. M. Riazi and A. Faghri, Gas absorption with zero-order chemical reaction, *A.I.Ch.E. Jl* **31,** 1967–1972 (1985).
4. M. Riazi and A. Faghri, Effect of interfacial drag on gas absorption with chemical reaction in a vertical tube, *A.I.Ch.E. Jl* **32,** 696–699 (1986).
5. M. Riazi and A. Faghri, Solid dissolution with zero-order chemical reaction, *Chem. Engng Sci.* **40,** 1601–1603 (1985).
6. G. Grossman and M. T. Heath, Simultaneous heat and mass transfer in absorption of gases in turbulent liquid films, *Int. J. Heat Mass Transfer* **27,** 2365–2376 (1984).
7. A. Faghri and R. A. Seban, Heat and mass transfer to a turbulent liquid film, *Int. J. Heat Mass Transfer* **31,** 891–894 (1988).
8. A. Faghri and R. A. Seban, Heat and mass transfer to a turbulent liquid film—II, *Int. J. Heat Mass Transfer* **32,** 1796–1798 (1989).
9. K. Suga and Boongorsrang, A new model of mass transfer in a rotating disk contactor, *Chem. Engng Sci.* **39,** 767–773 (1984).
10. R. N. Vaidya and V. G. Pangarkar, Predicting mass transfer rates in RBC for non-Newtonian fluids, *Water Res.* **23,** 1461–1464 (1989).
11. D. E. Bornside, C. W. Macosko and L. E. Scriven, Spin coating: one-dimensional model, *J. Appl. Phys.* **66,** 5186–5193 (1989).
12. S. Thomas, W. L. Hankey, A. Faghri and T. Swanson, One-dimensional analysis of hydrodynamic and thermal characteristics of thin film flows including the hydraulic jump and rotation, *ASME J. Heat Transfer* **112,** 728–735 (1990).
13. S. Thomas, A. Faghri and W. L. Hankey, Experimental analysis and flow visualization of a thin liquid film on a stationary and rotating disk, *ASME J. Fluids Engng* **113,** 73–80 (1991).
14. M. M. Rahman and A. Faghri, Numerical simulation of

fluid flow and heat transfer in a thin liquid film over a rotating disk, *Int. J. Heat Mass Transfer* **35**, 1441–1453 (1992).
15. M. Abramowitz and I. A. Stegun, *Handbook of Mathematical Functions with Formulas, Graphs and Mathematical Tables*. National Bureau of Standards, U.S. Department of Commerce, Washington, DC (1972).
16. W. A. Smith, *Elementary Numerical Analysis*. Prentice-Hall, Englewood Cliffs, New Jersey (1986).
17. S. V. Patankar, *Numerical Heat Transfer and Fluid Flow*. Hemisphere, New York (1980).
18. D. B. Spalding, Mathematical modeling of fluid mechanics, heat transfer and chemical reaction processes, a lecture course, CFDU HTS/80/1, Imperial College, London, U.K. (1980).
19. W. M. Kays and M. E. Crawford, *Convective Heat and Mass Transfer*, 2nd Edn. McGraw-Hill, New York (1980).